Strojniški vestnik - Journal of Mechanical Engineering vol(yyyy)no, p-p
Received for review: yyyy-mm-dd

Received revised form: yyyy-mm-dd
DOI code
Original / Review / Short Scientific Paper
Accepted for publication: yyyy-mm-dd

Studying the Effect of Thermal Fatigue on Multiple Cracks Propagating in SS316L Thin Flange on Shaft Specimen using Multi-Physics Numerical Simulation Model

Fariha Mukhtar[1], Faisal Qayyum[2], Hassan Elahi[3,*], Masood Shah[1], Khushboo Munir[4], Marco Eugeni[3], Paolo Gaudenzi[3]
[1] Department of Mechanical Engineering, University of Engineering and Technology, Taxila, Pakistan.
[2] Institut für Metallformung, Technische Universität Bergakademie Freiberg, Germany
[3] Department of Mechanical and Aerospace Engineering, Sapienza University of Rome, Italy
[4] DIET, Sapienza University of Rome, Italy

After more than a decade of research on thermal fatigue cracking in nuclear reactor components, the science is yet incomplete. It is important to understand the crack propagation behavior and the influence of multiple cracks on the fatigue life of a component due to thermal fatigue load. Accurate numerical simulation modeling can help in better understanding the influence of different factors on failure propagation. In this research a finite element based numerical simulation model has been developed using a commercial software ABAQUS to get the insight of crack propagation and crack arrest in SS316L thin flange on shaft specimen, the assembly is cooled internally and cyclic thermal loading is applied on the flange rim. The experimentation was carried out on a specially designed rig using induction coil for heating the outer rim is applied. Thermocouples were attached radially on the rim to collect detailed temperature profiles. Real-time temperature-dependent elastic-plastic material data was used for modeling. The boundary conditions and thermal profile used for the numerical model were matched with experimental data. The stresses responsible for crack initiation, the effect of crack number and crack lengths on stresses, energy absorbed at the crack tip after every thermal cycle and the threshold values of cracks are evaluated in the current work. The obtained simulation results were validated by comparing with experimental observations. The developed simulation model helps in better understanding the evolution of stresses and strains in uncracked and cracked SS316L disc mounted on a flange due to thermal cycling. It also helped in better understanding the crack propagation behavior and the evolution of energy release at crack tips. Such a model can help future researches in designing components undergoing thermal fatigue loading i.e. in nuclear power plants.

Keywords: Thermal fatigue, Numerical simulation, SS316L, Hoop Stress, Crack Propagation, J- integral

Highlights*:*

- Thermal loads occurring in nuclear power plants were used as boundary conditions.
- A detailed temperature-dependent material model of SS316L was used during the simulation.
- Crack initiation and propagation were observed to estimate the fatigue life of SS316L disc.
- Ratcheting behavior of SS316L results in plastic deformation and blunting of the crack tip.
- Developed numerical simulation model predictions correspond well with experimental observations.

0 INTRODUCTION

Nuclear power plants are designed for more than 40 years of service life [1] but due to the aggressive operational conditions, unforeseen environmental conditions and material behavior at elevated temperatures the overall service life of the plant is affected[2]. One such problem was encountered in the residual heat removal system of Civaux-1 power plant, France[3]. Due to higher toughness and superior corrosion resistance, austenitic stainless steels are used in the piping system of nuclear reactors[4]. AISI 321 is used in the secondary circuits of WWER (Water-Water Energetic Reactor) nuclear power plants and heat exchangers. SS304 and SS304L are frequently used in Pressurized Water Reactors[5]. SS316, SS316L, and SS316LN are mostly used in the piping system of LWR and LMFBR[6]. Although tough, these components undergo complex thermo-mechanical cycles during plant operations[7]. Varying temperatures in piping

*Corr. Author's Address: Department of Mechanical and Aerospace Engineering, Sapienza University of Rome, Via Eudossiana 18, 00184- Rome, Italy; hassan.elahi@uniroma1.it

systems due to thermal stratifications, turbulent mixing of the hot and cold fluid and vortex penetration in different regions of the system like mixing tees, joints, valves[8] result in thermal fatigue of such components[9]. Austenitic stainless steel can be largely affected by these thermal fluctuations because of their high thermal expansion coefficient and low fatigue endurance limit [10]. Mechanism of fatigue crack initiation and propagation is similar in the case of thermal and mechanical loading condition [11, 12]. Though thermal fatigue damage is proven to be more damaging than uniaxial isothermal fatigue [13, 14] both are administered by the same fatigue mechanism. Out of these multiple cracks, only dominant cracks grow faster[15]. Cracks may nucleate from the well-developed slip bands, punctual defects, inclusions, non-metallic impurities or surface imperfections[16]. These geometrical discontinuities are present due to the adopted manufacturing process [17] and act as crack initiation sites during service [18, 19]. The number of cycles to fatigue failure would significantly be decreased if the temperature is increased abruptly [20]. A fatigue crack when initiated grows slowly till the critical crack length is reached, after which the fatigue crack growth rate increases and leads to failure of the component. Due to lack of thermal fatigue test standard, different experimental arrangements are proposed by researchers for thermal fatigue testing of materials[12, 21]. Generally, researchers develop setups which are closer to actual conditions. For example, two- and three-dimensional loading condition SPLASH test facility and FAT3D [22]. Other researchers for thermal fatigue testing of austenitic stainless-steel grades 304L, 316L were carried out under different temperature ranges for evaluating the crack initiation and propagation in PWR and LMFBR conditions using SPLASH test facility [23].

Although several well-equipped experimental setups have been developed by researchers. It is still difficult and sometimes impossible to record critical material deformation and failure data while the test is in progress. Numerical simulation models developed in the past to study the fatigue life of metals[24], ceramics[25, 26] and polymers[27, 28] are helpful in understanding the material deformation and failure behavior under varying boundary and geometric conditions. They significantly contribute to reducing design cost and time.

Ullah et al. showed that numerical simulation models can help in better understanding the fatigue crack propagation in material under complex thermo-mechanical loading conditions[29]. Such models were also used to estimate the fatigue life of composite materials under dynamic loading conditions[30, 31]. Recently, based on elastic-plastic material data and realistic boundary conditions a method was developed by Qayyum et al. to numerically model the crack propagation in complicated structured due to thermal fatigue [15]. Such a model helps in successfully getting a deep insight into the complex thermal fatigue phenomena and therefore is adopted here.

In this research, a flange-shaft specimen made up of SS316L is experimentally tested under thermal fatigue loading provided by induction heating and internal cooling. The simulation was developed by incorporating real-time temperature-dependent elastic-plastic material data to get an insight into stress distribution and crack propagation in flange rim.

1 EXPERIMENTATION

The specimen consisted of a hollow shaft of SS316L on which a flange was machined as an integral part. Specimen geometry and dimensions are shown in Fig. 1(a). The idea behind using a thin flange is to have plane stress condition at the crack tip for easier analysis. The experimentation was carried out in collaboration with French partners at Ecole D’ Mines, Albi, France. The specimen was heated rapidly by 2 MHz high-frequency induction heating and cooled internally by flowing water at room temperature. 1 thermal cycle lasts for 16 seconds, with 4 seconds of heating and 12 seconds of subsequent cooling. The experimental arrangement is shown in Fig. 1(b).
The intended temperature profile was maintained and recorded with the help of spot-welded thermocouples at 0, 2.75 and 4.4mm from outer rim of flange. The temperature profile obtained from experimentation is shown in Fig. 2 with the help of solid lines.

Strojniški vestnik - Journal of Mechanical Engineering vol(yyyy)no, p-p

DOI code
Original / Review / Short Scientific Paper
Received for review: yyyy-mm-dd
Received revised form: yyyy-mm-dd
Accepted for publication: yyyy-mm-dd

2 NUMERICAL SIMULATION

ABAQUS Standard^{TM} is used as a Finite Element Analysis tool for the modeling and simulation of thermal fatigue. In this analysis, a de-coupled thermo-mechanical approach is used with non-linear rate-independent elastic-plastic material model as suggested by Fissolo et al [13].

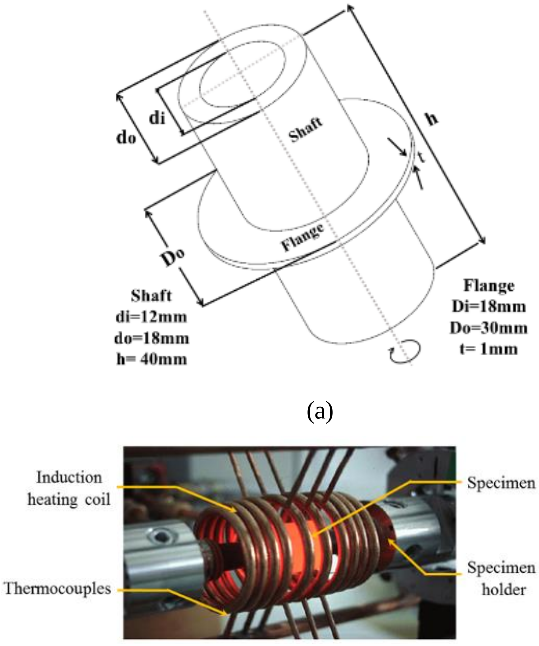

(b)

Fig. 1. *Experimentation (a) Specimen geometry (b) Induction heating of the specimen [31]*

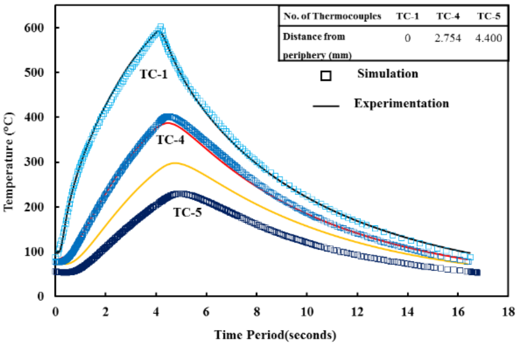

Fig. 2. *Thermal profile matching with the description of thermocouple positioning*

2.1 Material data

SS316L is a non-hardenable and non-magnetic grade of stainless steel. It is used where toughness and corrosion resistance are equally important [10]. Temperature-dependent material properties of SS316L which are listed in Table 1 were incorporated in the numerical simulation model. The flow curves of the material at different temperatures are presented in Fig. 3. This temperature dependent elastic-plastic material data was used in numerical model definition.

Table 1. *Temperature dependent Mechanical Properties of SS316L [32]*

Temp (°C)	Young's Modulus (GPa)	Thermal Conduct. (W/mm.K)	Therm. Exp. Coef. (1e-5/°C)	Specific heat (kJ/kg.K)
25	200	0.014	1.60	464.68
100	194	0.0149	1.66	----
200	185	0.016	----	----
300	177	0.0173	----	----
400	169	0.0186	----	515.6
500	160	0.0199	----	----
800	135	0.02		569.2
871	-----	----	1.98	----

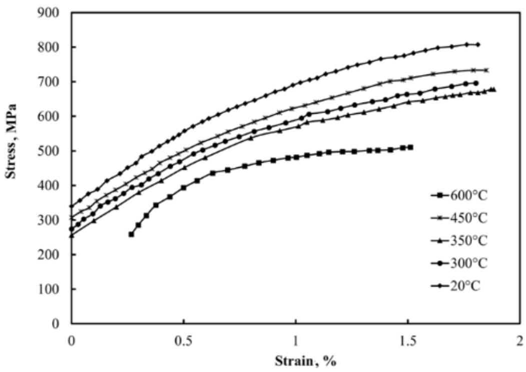

Fig. 3. *Temperature-dependent Plasticity data of SS316L [32]*

2.2 Loading and Constraints

Thermal heat flux of 2 W/mm^2 was applied at the rim of the disc in all simulation models. The temperature profiles at different depths in the numerical simulation model were matched with experimentally observed profiles by tuning the amplitude of heat flux and cooling. The simulation was run for 30 fatigue cycles to get stabilized

*Corr. Author's Address: Department of Mechanical and Aerospace Engineering, Sapienza University of Rome, Via Eudossiana 18, 00184- Rome, Italy; hassan.elahi@uniroma1.it

stress-strain response. The boundary conditions defined for all simulations models are shown in Fig. 4(a). Pinned boundary condition was applied at the internal periphery of the shaft. Element type DC2D4 (4-node linear heat transfer quadrilateral) was used to generate a total of 4260 linear quadrilateral elements on the whole assembly. The meshed assembly of disc and shaft is shown in Fig. 4(b). The model was checked for the mesh dependency and during meshing the aspect ratio (which is a measure of how well structured the mesh is i.e. Perfect aspect ratio is 1.0) was maintained below 1.05. To get more details about the numerical simulation model development, meshing, boundary conditions and post-processing of data, readers are encouraged to read the previous publications[33, 34].

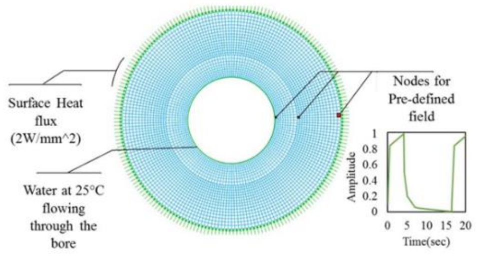

(a)

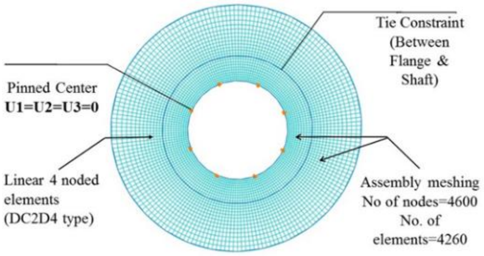

(b)

Fig. 4. *Loading and constraints (a) Heating Model Specifications, (b) Mechanical model specifications*

2.3 Mechanical Model

A total of 29 models were developed for this research with different crack lengths and number of cracks. The simulations were based on the sequence published earlier [12, 35]. To get nodal temperature distributions, a thermal analysis was run and the temperature evolution at each node was recorded. A model was developed to study the effect of thermal cycling on the uncracked sample which results in highest hoop stresses. 27 models with different crack numbers and crack lengths were analyzed to study the effect of varying crack number and crack length on evolving stresses at the periphery of the disc. Description of peripheral cracks is shown in Fig. 5.

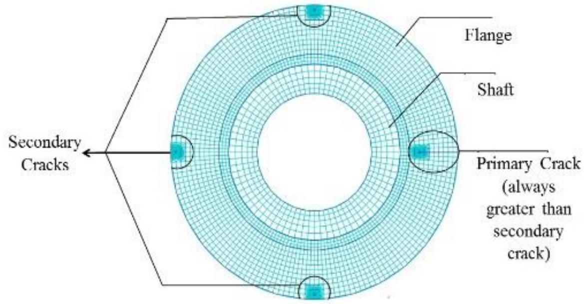

Fig. 5. *Description of Peripheral Cracks in the Specimen*

3 RESULTS

Experimentally it is observed that two diametrically opposite cracks initiate at the outer periphery of the flange. Cracks initiate in the flange after 6000 thermal cycles. The two cracks originated were 180° apart from each other as shown in Fig. 6(b). The same phenomenon of cracking was observed previously in the case of H-11 tool steel disc[15]. In case of H-11 tool steel, multiple cracks originated on the periphery, out of which only 8 cracks propagated throughout the experiment which was validated through numerical simulation, whereas in this case only two noticeable cracks initiated and propagated up to 16000 cycles. One of the cracks propagated to a crack length of 1640 μm and the other grew up to 825 μm for the same number of cycles. Number of cycles to crack initiation and the significant crack lengths attained by the two cracks is shown in Fig. 6(b).

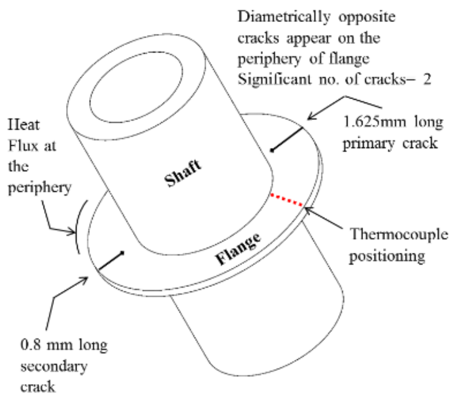

(a)

Strojniški vestnik - Journal of Mechanical Engineering vol(yyyy)no, p-p

DOI code
Original / Review / Short Scientific Paper
Received for review: yyyy-mm-dd
Received revised form: yyyy-mm-dd
Accepted for publication: yyyy-mm-dd

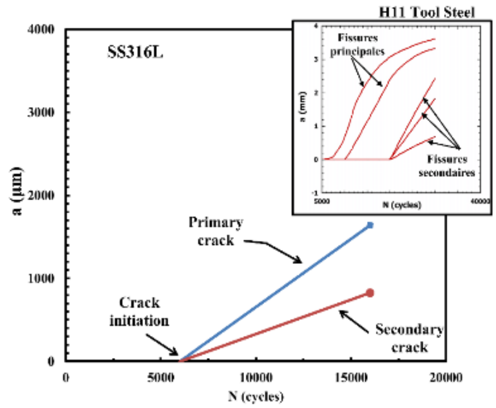

(b)

Fig. 6. *Experimental results (a) no. of cycles to cr ack initiation, (b) diametrically opposite cracks as a result of thermal fatigue*

3.1 Temperature- Stress correspondence

Maximum hoops stress is observed at the rim of the flange. The change in hoop stress versus temperature when plotted forms a hysteresis loop as shown in Fig. 7, area under the hysteresis is representing the energy absorbed by the material itself to reach the peak stress with the increase in temperature. The first cycle (from 0 to 1) shows a sudden increase in stress with increasing the temperature. Compressive stresses develop in the disc (from 1 to 2) when the temperature is raised while they start to transform into tensile stresses (from 2 to 3) during the cooling period. Tensile stress reaches a maximum magnitude of 396MPa in the last cycle at point 4 which shows a 21% increase in stress as compared to the 1st cycle. These stresses are responsible for the crack initiation in the disc. When 1st and last cycle compressive stresses are compared, 13.4% elevation is observed at point 2.

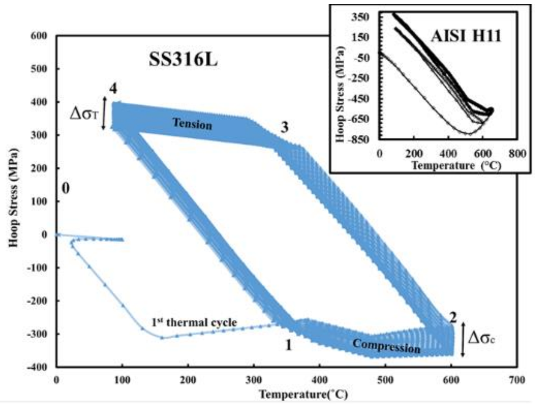

Fig. 7. *Stress-temperature hysteresis of SS316L and H11 tool steel (for comparison)*

3.2 Effect of crack lengths and number of cracks on Hoop Stress

Maximum hoops stress is observed on the rim of the flange. The variation in hoop stress on the rim due to cracking forms plateaus of hoop stresses which are presented in Fig. 8. In this figure, n is the number of cracks, a_p is the length of the primary crack, a_s is the length of the secondary crack. The graph shows that hoop stress suddenly falls when a crack is introduced in the specimen. The initiation of the crack and its opening in the cooling cycle results in stress-relieving. An increasing number of cracks results in an overall decrease in hoop stress on the rim. By comparing Fig. 8(a) with Fig. 8(b) it is observed that introducing a crack causes sudden stress relaxation at the respective point on the rim.

In the case of SS316L disc, only two cracks initiate and propagate to significant lengths during the experimentation. This validates the numerical simulation results in which a 7% drop in hoop stress is recorded when the crack number increases from 2 to 4 i.e. from Fig. 8(b) to Fig. 8(c).

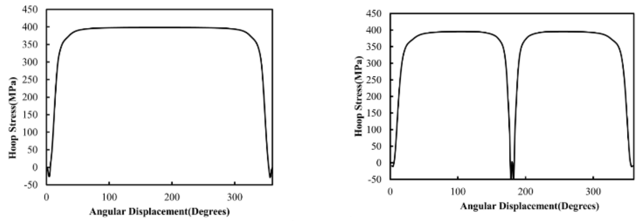

(a) n=1, a_p=2mm, a_s=0mm

(b) n=2, a_p=2mm, a_s=1mm

*Corr. Author's Address: Department of Mechanical and Aerospace Engineering, Sapienza University of Rome, Via Eudossiana 18, 00184- Rome, Italy; hassan.elahi@uniroma1.it

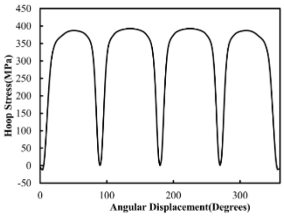

(c) n=4, a_p=2mm, a_s=1mm

Fig. 8. *Distribution of Hoop Stress along the periphery of SS316L disc with different no. of cracks*

In Fig. 9 secondary crack length is plotted as a function of hoop stress for different primary crack lengths. For every set of primary crack length i.e. 2mm, the hoop stress decreases with an increase in secondary crack length, same goes for the set where primary crack length is kept 3mm and 4mm respectively. For a 2mm secondary crack, hoop stress has a maximum value of 396 MPa. The minimum value of hoop stress for n=4 is recorded when the primary crack length is 4mm and secondary crack length is 3mm.

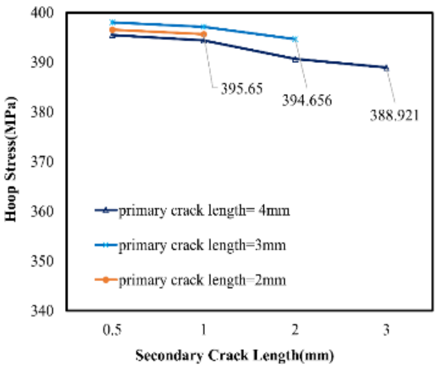

(a)

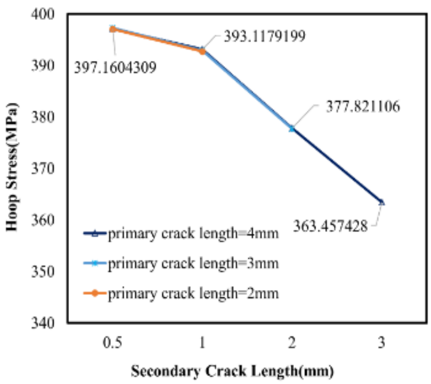

(b)

Fig. 9. *Maximum hoop stress as a function of secondary crack length (a) for n=2, (b) for n=4*

3.3 Crack propagation phenomenon

Anderson [36] has explained in his book that either J-integral or CTOD can be used as a fracture criterion for time-independent, elastic-plastic behavior of materials that are to be dealt with in non-linear Elastic-Plastic Fracture Mechanics. Both J-integral and CTOD gives information about the crack- tip condition. Researchers have also associated the fatigue crack growth to the cyclic J-integral [37]. Time response of J-integral resulted in spikes as shown in Fig. 10. Spikes are formed as a result of sudden rise and fall in the values of J-integral, which is governed by continuous thermal cycling of the flange. During the tension cycle, the crack opens which results in the release of energy while in the compression cycle crack remain closed hence no energy is being released. This release in energy results in crack propagation during the cooling cycle. The j-integral trend, in this case, is comparatively different from that observed in the case of H-11 tool steel. Although the spikes formed in case of H-11 tool steel were comparable to that of SS316L J-integral does not get stabilized with subsequent thermal cycling in SS316L, the values seem shifted from the horizontal axis.

The graph is shown in Fig. 11, is the response of CMOD with respect to time. CMOD increases with time after every cycle. It is maximum at the instance where tensile stress is maximum i.e. at the end of every thermal cycle. The overall shift in the value of CMOD from horizontal axis represents the cumulative plastic deformation at the crack tip which is adding a certain value to its displacement response taken for last 12 cycles.

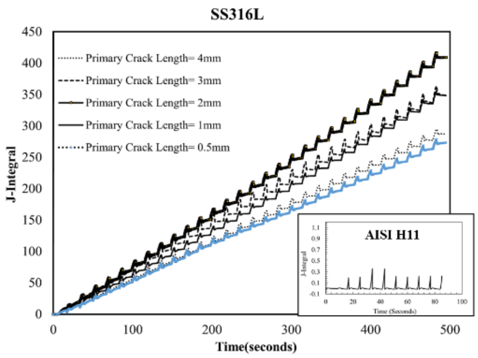

Fig. 10. *J-Integral Vs Time; For n=1; inserted graph: J-integral vs time for n=1 & ap=2mm*

Strojniški vestnik - Journal of Mechanical Engineering vol(yyyy)no, p-p

DOI code
Original / Review / Short Scientific Paper
Received for review: yyyy-mm-dd
Received revised form: yyyy-mm-dd
Accepted for publication: yyyy-mm-dd

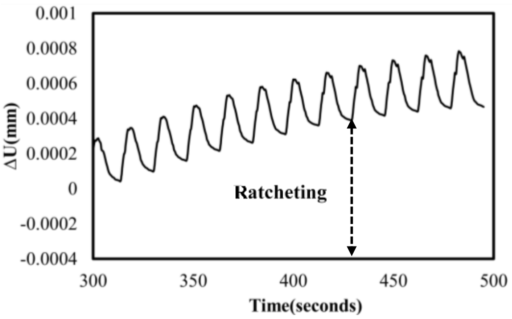

Fig. 11. *CMOD Vs Time for last 12 cycles,n=1, ap= 1mm*

4 DISCUSSION

Maximum hoop stress is observed on the rim of the flange. The hoop stress is compressive during heating, reduces to zero and eventually becomes tensile during cooling due to retained plasticity. In this research, these stresses were analyzed using calibrated thermal and mechanical models and were observed that an energy hysteresis is observed in the case of SS316L with increasing area. Which shows that there is continuous energy absorption at the crack tip.

The crack initiation was not the main focus in this research but has been previously investigated to occur due to dislocations accumulation at grain boundaries, or inclusions or voids to form micro-cracks which eventually join together to form bigger crack which grows to larger extends under the influence of tensile stresses.

During each thermal cycle, a complex phenomenon occurs at the crack tip. This research was carried out to see and understand this phenomenon in a better way. In the first thermal cycle during heating, the material softens and compressive hoop stresses accumulate on the rim of the flange and the crack faces close, as shown in Fig. 12(a). Tensile hoop stresses originate during cooling which is responsible for crack opening, as can be observed in Fig. 12(b).

It is observed in this research that during cyclic thermal loading stainless steel undergoes ratcheting behavior. Energy absorption at crack tip results in crack tip blunting and with subsequent thermal cycles the crack tip does not close even at the highest temperature. This can be seen for the 5th cycle in Fig. 12 (c,d) and for the 30th cycle in Fig. 12 (e,f).

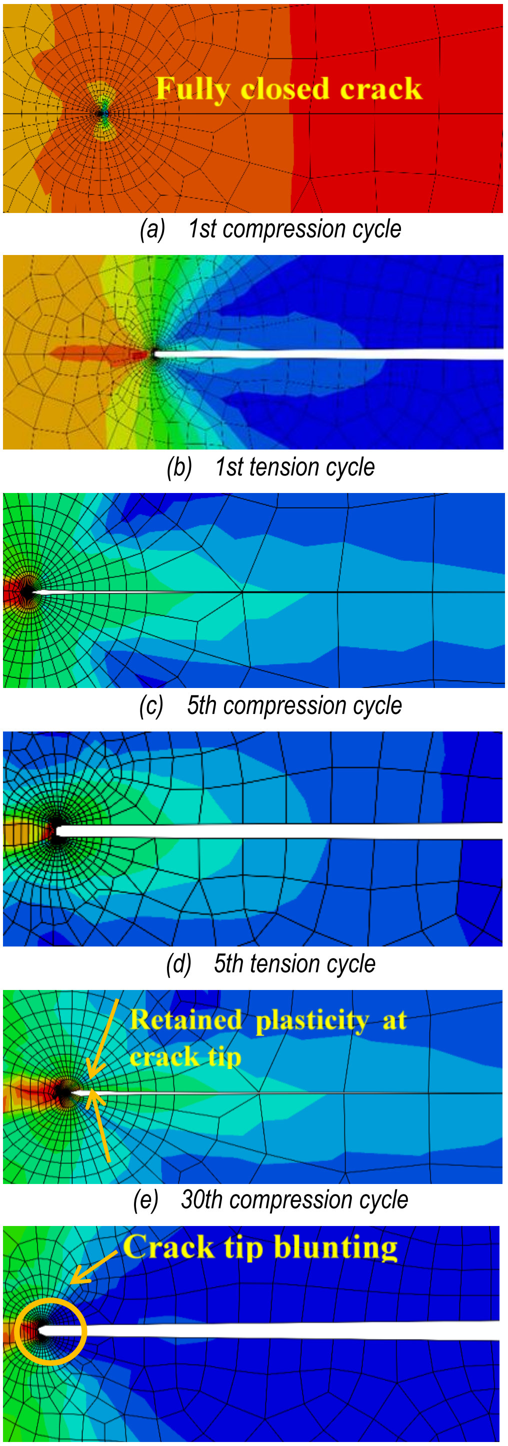

(a) 1st compression cycle

(b) 1st tension cycle

(c) 5th compression cycle

(d) 5th tension cycle

(e) 30th compression cycle

(f) 30th tension cycle

Fig. 12. *Crack tip condition in subsequent cycles*

J integral shows an increasing trend with the increase in crack length in Fig. 10. J- Integral reaches its maximum value after 30 cycles. It is

*Corr. Author's Address: Department of Mechanical and Aerospace Engineering, Sapienza University of Rome, Via Eudossiana 18, 00184- Rome, Italy; hassan.elahi@uniroma1.it

observed that J- Integral increases with an increase in crack length up to 2mm. There is 15.33% increase in energy release rate when the crack grows from 1mm to 2mm. On further increasing the crack length up to 3mm the maximum value of the energy release rate was approximately the same as that for a crack length of 1mm. On further increase in crack length from 2mm to 3mm and 4mm, 15.34% and 29% drop in corresponding values of J-integral is recorded.

Crack Mouth Opening Displacement and crack tip opening displacement are the two parameters which are also used to estimate the crack growth rate. Researchers have associated the fatigue crack propagation to the CMOD[38]. As CMOD increases with an increase in crack length as shown in Fig. 11. 0.61% decrease in hoop stress is observed where the number of cracks remains the same while secondary crack length increases from 1mm to 2mm. For both the cases i.e. n=2 and n=4, CMOD increases with an increase in secondary crack length. An overall decrease can be seen in Fig. 11, when n=4 which points towards the limitation of the number of cracks on the periphery. Fig. 11 shows that CMOD increases with an increase in primary crack length. The relationship curve between primary crack length and CMOD for n=4 overlaps with n=2. It shows that for greater crack length, CMOD will be greater independent of the number of cracks.

5 CONCLUSIONS

In this research, a cracked and un-cracked flange-shaft specimen of SS316L was numerically simulated using the elastic-plastic material model with isotropic hardening in Mode-I fracture. The simulation was based on the results obtained by the experimentation of the disc type specimen of SS316L under thermal cyclic loading provided by the induction heating and internal cooling. The experimentation resulted in two diametrically opposed cracks which propagated to 1640 µm and 825 µm in length. The results of the numerical simulation give the agreeable validation of the experimentation. The obtained results can be concluded as follows:

o Material permanently deforms in 1st thermal cycle. During thermal cycling, stress reverses itself and results in a stress-strain hysteresis. The pair of stresses develop in the specimen exceed the fatigue endurance limit of the material.

o Hoop stress on the flange stands responsible for crack initiation in it, when the number of cracks is increased from n=2 to n=4, a maximum drop of 6.4% in hoop stress is recorded which justifies the two-crack formation phenomenon during experimentation.

o J-integral gave us the possible range of primary crack length which is 0.5≦ap≦2.5mm while there is enough energy available in the specimen to drive the secondary crack up to 2mm.

o CMOD increases regardless of the number of cracks or cracks length, thus cannot be relied on as a good identifier of thermal fatigue damage.

o Time response of J-integral and CMOD points towards the ratcheting behavior of SS316L and crack blunting in the specimen.

7 NOMENCLATURE

PWR	: Pressurized Water Reactor
LMFBR	: Liquid Metal Fast Breeder Reactor
LWR	: Light Water Reactor
CMOD	:Crack mouth opening displacement
n	: Number of cracks
N	: Number of cycles
a	: Crack length
as	: Secondary crack length
ap	: Primary crack length
CTOD	: Crack tip opening displacement
U1	: Displacement in X-direction
U2	: Displacement in Y-direction
U3	: Displacement in Z-direction

8 REFERENCES

[1] Le Duff, J.-A., Ould, P., Bernard, J.-L. (1996). Fatigue crack initiation and propagation in austenitic stainless steels for light water reactors. *International journal of pressure vessels and piping,* vol. 65, no. 3, p. 241-253.

[2] Paffumi, E., Nilsson, K.-F., Szaraz, Z. (2015). Experimental and numerical assessment of thermal fatigue in 316 austenitic steel pipes. *Engineering Failure Analysis,* vol. 47, p. 312-327.

DOI code
Original / Review / Short Scientific Paper
Received for review: yyyy-mm-dd
Received revised form: yyyy-mm-dd
Accepted for publication: yyyy-mm-dd

[3] Cipiere, M., Le Duff, J. (2002). Thermal fatigue experience in french piping: Influence of surface condition and weld local geometry. *Welding in the World,* vol. 46, no. 1-2, p. 23-27.

[4] Avner, S.H. (1974). *Introduction to physical metallurgy*. McGraw-hill New York,

[5] Kadlec, M., Haušild, P., Siegl, J., Materna, A., Bystrianský, J. (2012). Thermal fatigue crack growth in stainless steel. *International Journal of Pressure Vessels and Piping,* vol. 98, p. 89-94.

[6] Reddy, G.P., Kannan, R., Mariappan, K., Sandhya, R., Sankaran, S., Rao, K.B.S. (2015). Effect of strain rate on low cycle fatigue of 316ln stainless steel with varying nitrogen content: Part-i cyclic deformation behavior. *International Journal of Fatigue,* vol. 81, p. 299-308.

[7] Wang, Y., Charbal, A., Hild, F., Vincent, L. (2018). High cycle thermal fatigue of austenitic stainless steel. *MATEC Web of Conferences*, p. 19009.

[8] Paffumi, E., Nilsson, K.-F., Taylor, N. (2008). Simulation of thermal fatigue damage in a 316l model pipe component. *International Journal of Pressure Vessels and Piping,* vol. 85, no. 11, p. 798-813.

[9] Zhan, J., Li, M., Huang, J., Bi, H., Li, Q., Gu, H. (2019). Thermal fatigue characteristics of type 309 austenitic stainless steel for automotive manifolds. *Metals,* vol. 9, no. 2, p. 129.

[10] McGuire, M.F. (2008). *Stainless steels for design engineers*. Asm International,

[11] Qayyum, F., Kamran, A., Ali, A., Shah, M. (2017). 3d numerical simulation of thermal fatigue damage in wedge specimen of aisi h13 tool steel. *Engineering Fracture Mechanics,* vol. 180, p. 240-253, DOI: https://doi.org/10.1016/j.engfracmech.2017.05.020.

[12] Elahi, H., Eugeni, M., Gaudenzi, P., Qayyum, F., Swati, R.F., Khan, H.M. (2018). Response of piezoelectric materials on thermomechanical shocking and electrical shocking for aerospace applications. *Microsystem Technologies,* vol. 24, no. 9, p. 3791-3798.

[13] Fissolo, A., Amiable, S., Ancelet, O., Mermaz, F., Stelmaszyk, J., Constantinescu, A., Robertson, C., Vincent, L., Maillot, V., Bouchet, F. (2009). Crack initiation under thermal fatigue: An overview of cea experience. Part i: Thermal fatigue appears to be more damaging than uniaxial isothermal fatigue. *International Journal of Fatigue,* vol. 31, no. 3, p. 587-600.

[14] Swati, R., Wen, L., Elahi, H., Khan, A., Shad, S. (2019). Experimental and numerical investigation of transversal damage in carbon fiber reinforced composites using x-fem analysis. *Journal of Mechanical Science and Technology,* vol. 33, no. 1, p. 205-211.

[15] Qayyum, F., Shah, M., Shakeel, O., Mukhtar, F., Salem, M., Rezai-Aria, F. (2016). Numerical simulation of thermal fatigue behavior in a cracked disc of aisi h-11 tool steel. *Engineering Failure Analysis,* vol. 62, p. 242-253, DOI: https://doi.org/10.1016/j.engfailanal.2016.01.015.

[16] Mukhtar, F., Qayyum, F., Anjum, Z., Shah, M. (2019). Effect of chrome plating and varying hardness on the fretting fatigue life of aisi d2 components. *Wear,* vol. 418-419, p. 215-225, DOI: https://doi.org/10.1016/j.wear.2018.12.001.

[17] Klesnil, M., Lukác, P. (1992). *Fatigue of metallic materials*. Elsevier,

[18] Kerezsi, B.B., Price, J.W. (2002). Using the asme and bsi codes to predict crack growth due to repeated thermal shock. *International journal of pressure vessels and piping,* vol. 79, no. 5, p. 361-371.

[19] Swati, R., Elahi, H., Wen, L., Khan, A., Shad, S., Mughal, M.R. (2018). Investigation of tensile and in-plane shear properties of carbon fiber reinforced composites with and without piezoelectric patches for micro-crack propagation using extended finite element method. *Microsystem Technologies,* vol., p. 1-10.

[20] Srivastava, A., Joshi, V., Shivpuri, R. (2004). Computer modeling and prediction of thermal fatigue cracking in die-casting tooling. *Wear,* vol. 256, no. 1-2, p. 38-43.

[21] Memmolo, V., Elahi, H., Eugeni, M., Monaco, E., Ricci, F., Pasquali, M., Gaudenzi, P. (2019). Experimental and numerical investigation of pzt response in composite structures with variable degradation levels. *Journal of Materials Engineering and Performance,* vol., p. 1-8.

*Corr. Author's Address: Department of Mechanical and Aerospace Engineering, Sapienza University of Rome, Via Eudossiana 18, 00184- Rome, Italy; hassan.elahi@uniroma1.it

[22] Khan, M. U., Butt, Z., Elahi, H., Asghar, W., Abbas, Z., Shoaib, M., & Bashir, M. A. (2018). Deflection of coupled elasticity–electrostatic bimorph PVDF material: theoretical, FEM and experimental verification. Microsystem Technologies, 1-8.

[23] Amiable, S., Chapuliot, S., Constantinescu, A., Fissolo, A. (2006). A comparison of lifetime prediction methods for a thermal fatigue experiment. *International Journal of Fatigue,* vol. 28, no. 7, p. 692-706.

[24] Wang, Y., Charbal, A., Hild, F., Roux, S., Vincent, L. (2019). Crack initiation and propagation under thermal fatigue of austenitic stainless steel. *International Journal of Fatigue,* vol. 124, p. 149-166.

[25] Elahi, H., Eugeni, M., Gaudenzi, P. (2019). Design and performance evaluation of a piezoelectric aeroelastic energy harvester based on the limit cycle oscillation phenomenon. *Acta Astronautica,* vol. 157, p. 233-240.

[26] Butt, Z., Anjum, Z., Sultan, A., Qayyum, F., Ali, H.M.K., Mehmood, S. (2017). Investigation of electrical properties & mechanical quality factor of piezoelectric material (pzt-4a). *Journal of Electrical Engineering & Technology,* vol. 12, no. 2, p. 846-851.

[27] Najabat Ali, M., Ansari, U., Sami, J., Qayyum, F., Mir, M. (2016). To develop a biocompatible and biodegradable polymer-metal composite with good; mechanical and drug release properties. *J Mater Sci Eng,* vol. 5, no. 274, p. 2169-0022.10002.

[28] Mir, M., Ali, M.N., Ansari, U., Smith, P.J., Zahoor, A., Qayyum, F., Abbas, S. (2019). Aqua-gel ph sensor: Intelligent engineering and evaluation of ph sensor based on multi-factorial testing regimes. *Sensor Review,* vol. 39, no. 2, p. 178-189.

[29] Ullah, M., Pasha, R.A., Chohan, G.Y., Qayyum, F. (2015). Numerical simulation and experimental verification of cmod in ct specimens of tig welded aa2219-t87. *Arabian Journal for Science and Engineering,* vol. 40, no. 3, p. 935-944, DOI: 10.1007/s13369-015-1569-1.

[30] Asghar, W., Nasir, M.A., Qayyum, F., Shah, M., Azeem, M., Nauman, S., Khushnood, S. (2017). Investigation of fatigue crack growth rate in carall, arall and glare. *Fatigue & Fracture of Engineering Materials & Structures,* vol. 40, no. 7, p. 1086-1100, DOI: 10.1111/ffe.12566.

[31] Swati, R., Wen, L., Elahi, H., Khan, A., Shad, S. (2019). Extended finite element method (xfem) analysis of fiber reinforced composites for prediction of micro-crack propagation and delaminations in progressive damage: A review. *Microsystem Technologies,* vol. 25, no. 3, p. 747-763.

[32] Kim, J.-B., Lee, H.-Y., Park, C.-G., Lee, S.-H., Lee, J.-H. (2005). The temperature dependent inelastic material characteristics of cold worked 316l for nonsta. *Proc. of the KNS,* vol.

[33] Anjum, Z., Qayyum, F., Khushnood, S., Ahmed, S., Shah, M. (2015). Prediction of non-propagating fretting fatigue cracks in ti6al4v sheet tested under pin-in-dovetail configuration: Experimentation and numerical simulation. *Materials & Design,* vol. 87, p. 750-758.

[34] Qayyum, F., Shah, M., Manzoor, S., Abbas, M. (2015). Comparison of thermomechanical stresses produced in work rolls during hot and cold rolling of cartridge brass 1101. *Materials Science and Technology,* vol. 31, no. 3, p. 317-324, DOI: 10.1179/1743284714Y.0000000523.

[35] Khan, F., Qayyum, F., Asghar, W., Azeem, M., Anjum, Z., Nasir, A., Shah, M. (2017). Effect of various surface preparation techniques on the delamination properties of vacuum infused carbon fiber reinforced aluminum laminates (carall): Experimentation and numerical simulation. *Journal of Mechanical Science and Technology,* vol. 31, no. 11, p. 5265-5272, DOI: 10.1007/s12206-017-1019-y.

[36] Anderson, T.L. (2005). *Solutions manual for fracture mechanics: Fundamentals and applications*. Taylor & Francis,

[37] Sadananda, K., Shahinian, P. (1980). *Fracture mechanics*, ASTM International

[38] Schweizer, C., Seifert, T., Nieweg, B., Von Hartrott, P., Riedel, H. (2011). Mechanisms and modelling of fatigue crack growth under combined low and high cycle fatigue loading. *International journal of fatigue,* vol. 33, no. 2, p. 194-202.